CLM-P761

CLM-P761

UKAEA

Preprint

PLASMA EDGE PHYSICS FOR NET/INTOR

M. F. A. HARRISON
E. S. HOTSTON

CULHAM LABORATORY
Abingdon Oxfordshire
1985

CLM-P 761

PLASMA EDGE PHYSICS FOR NET/INTOR

M.F.A. Harrison and E.S. Hotston
Culham Laboratory, Abingdon, Oxon OX14 3DB, U.K.
(UKAEA/Euratom Fusion Association)

in collaboration* with

A. De Matteis
ENEA, Instituto di Bologna

ABSTRACT

The boundary plasma of NET/INTOR has been modelled using a two-dimensional fluid description of the plasma. The region modelled extends from the inner to the outer single-null divertor channels via the scrape-off plasma. It also includes a thin layer of plasma inboard of the separatrix. Transport of recycling neutral particles is treated in a simplified manner which neglects molecules but the results are in general accord with more detailed analyses based on a Monte Carlo treatment.

The results show that the power flow to the divertor channels is asymmetric and that the peak power loading at the outer target (if the target is located normally to the magnetic surfaces) is about 20 MW/m^2. High recycling within the divertor reduces the peak electron temperature of the plasma sheath to 29 eV at the outer and 9 eV at the inner targets respectively. Sputtering of the tungsten target is very modest, about 10^{19} atom/s. This corresponds to 9 mm/a erosion (for 100% availability and for a target located normally to the magnetic surfaces) but the net erosion is expected to be substantially less because of the redeposition of sputtered atoms. Uncontrolled motion of the divertor plasma across the target is also expected to reduce net erosion. Pumping of helium can be optimised by restricting the height of the pumping ducts to about 0.25 m. Some backflow of DT plasma from the throats of the high recycling divertor is predicted and this may degrade the exhaust of helium.

(Report on work carried out under Contract No. 133/83-9/FU-UK/NET)

* This aspect of the work forms part of Contract No. 153/84-4/FU-I/NET but is reported here because of its close relevance to the subject under discussion.

September 1985

1. INTRODUCTION

Present concepts of plasma composition control in NET require solutions of physics problems which are similar to those encountered in INTOR. Typical requirements are: (a) about 2 x 10^{20} helium atoms/s must be pumped from the tokamak in order to maintain the concentration of helium ash within the fusion plasma at about 5%, (b) non-radiated power transported by the boundary plasma is probably 80 MW and (c) the concentration of heavy impurity species within the fusion plasma should not exceed ~ 10^{-4}. Previous studies of NET and INTOR had established by mid 1983 that the most attractive solutions will probably be based on the poloidal divertor concept which is envisaged to be an open throated, single-null configuration. Furthermore, the divertor should operate in the high recycling regime. The advantages of this mode of operation derive from the large flux of plasma particles which is incident upon the divertor target. This minimises the particle pumping requirements for helium and it ensures that the plasma adjacent to the target has a temperature of only a few tens of electron volts. At such modest temperatures the energy of the incident plasma ions barely exceeds the sputtering threshold for high atomic number materials (for example, tungsten) so that the sputtering rate of such impurities is low. The operational lifetime of the target is then likely to be several years even when redeposition of sputtered material is neglected. Moreover, backflow of sputtered impurity ions into the edge of the main plasma can be kept to reasonable limits without invoking the need for a high degree of retention of impurity ions within the confines of the divertor chamber.

These early predictions are based upon one-dimensional modelling of plasma transport in the direction parallel to the magnetic field. Transport transverse to the field within the scrape-off and divertor plasma is accounted for only by means of prescribed radial profiles which are taken from the nominal operating conditions quoted for INTOR (see Refs. 1 and 2). Analyses in which the radial profile of the scrape-off layer has been more consistently related to the radial conduction of energy[3] show clearly that the prescribed profiles are too narrow and that the power loading (and probably the peak plasma temperature adjacent to the target[4]) are likely to be higher than previously envisaged. However, these quasi-two-dimensional approaches do not include particle convection which, to some extent, has a

beneficial effect. It was therefore highly desirable to evolve a detailed two-dimensional model for plasma transport which is linked to a two-dimensional analysis of recycling and neutral particle pumping. This task has been the main component of work carried out under NET Contract 133/83-9/FU-UK/NET.

Plasma modelling is based upon a two-fluid description of electrons and D/T ions and the transport is described by Braginskii equations. These equations are numerically solved using a computational code previously developed by Braams[5] and the objective of the present study has been to apply this code to the geometry and recycling conditions foreseen for the edge plasma of NET/INTOR. Preliminary results of the study were contributed to the January 1984 INTOR Workshop[6] but at this time the analysis dealt only with the boundary plasma layer which feeds the outer divertor target and moreover only in the region outboard of the separatrix. The analysis was subsequently extended to include the divertor plasma inboard of the separatrix (Ref. 7) and finally, in the contribution to the October INTOR Workshop[8], it embraced the full geometry of both the inner and outer divertor targets together with the connecting scrape-off plasma. The present NET report is based upon the work in Ref. 8 but it has been substantially updated in order to eliminate certain inconsistencies and also to benefit from improvements in modelling.

Throughout the study it has been important that there be confluent advances in modelling of plasma and of recycling neutral D/T particles. Precise analyses of neutral transport based on the NIMBUS three-dimensional Monte Carlo code are being persued at ENEA Bologna and, because transport of neutrals and plasma is strongly interactive, very close collaboration is maintained with Culham. A previous collaborative study[9] provides preliminary information on helium exhaust and sputtering damage for a divertor in NET or INTOR. However, this is based upon a simplified one-dimensional plasma model and more consistent linking of neutral and plasma transport in the realistic geometry of the NET design is needed to establish a better physics specification of the divertor.

Progress in this direction has been greatly hindered by the difficulties in obtaining converged numerical solutions from the plasma code for conditions where the ions recycle many times (more than ~ 50) to the divertor target. Recent results show that this problem has now been

solved but it has not yet been practicable to link the two codes in a fully consistent manner. Nevertheless, throughout the study it has been possible to make the plasma code converge by invoking simpler models of recycling which include only approximate spatial distributions of ionisation sources and radiative power losses due to hydrogen atoms. These models neglect molecular effects and energy lost to the walls by charge exchange. In view of the stringent schedule of NET/INTOR contributions, such simplistic approaches have perforce been adopted. Results derived from the two-dimensional plasma code with simplified recycling have also been used as input for the NIMBUS Monte Carlo code and applied to the NET and INTOR geometry in order to update the specifications for pumping and for sputtering damage. It is considered that deviation from self-consistent linking of the models is so small that only modest errors are present in the results for neutral particle transport. These data from NIMBUS derive from work carried out under NET Contract 153/84-4/FU-I/NET but are reported here because of their close relevance to plasma modelling.

2. PLASMA MODELLING

2.1 The Fluid Model

The description of transport within the scrape-off and divertor regions is based upon a two-fluid treatment of the plasma electrons and ions. Two-dimensional Braginskii equations are used to describe transport in the directions parallel and transverse to the magnetic field. The numerical code used to solve these equations has been developed by Braams[5]. A pseudo-rectangular geometry is adopted in which the x-axis lies parallel to the magnetic field and the y-axis lies in the transverse (i.e. radial) direction. In steady state conditions the following system of equations governs the ion density n_i, the parallel flow velocity u, the radial diffusion velocity v, and the temperatures T_e and T_i.

Continuity:

$$\frac{1}{\sqrt{g}} \frac{\partial}{dx} \left(\frac{\sqrt{g}}{h_x} n_i u\right) + \frac{1}{\sqrt{g}} \frac{\partial}{\partial y} \left(\frac{\sqrt{g}}{h_y} n_i v\right) = S_n \qquad (2.1)$$

Momentum balance:

$$\frac{1}{\sqrt{g}} \frac{\partial}{\partial x} \left(\frac{\sqrt{g}}{h_x} \rho u^2 - \frac{\sqrt{g}}{h_x^2} \eta_x^i \frac{\partial u}{\partial x} \right) + \frac{1}{\sqrt{g}} \frac{\partial}{\partial y} \left(\frac{\sqrt{g}}{h_y} \rho vu - \frac{\sqrt{g}}{h_y^2} \eta_y^i \frac{\partial u}{\partial y} \right)$$

$$= S_{mu} - \frac{1}{h_x} \frac{\partial}{\partial x} p \qquad (2.2)$$

Radial diffusion:

$$v = - \frac{D}{h_y} \frac{\partial}{\partial y} (\ell n \, n_i) \qquad (2.3)$$

Electron energy balance:

$$\frac{1}{\sqrt{g}} \frac{\partial}{\partial x} \left(\frac{\sqrt{g}}{h_x} \frac{5}{2} n_e u T_e - \frac{\sqrt{g}}{h_x^2} \kappa_x^e \frac{\partial}{\partial x} T_e \right)$$

$$+ \frac{1}{\sqrt{g}} \frac{\partial}{\partial y} \left(\frac{\sqrt{g}}{h_y} \frac{5}{2} n_e v T_e - \frac{\sqrt{g}}{h_y^2} \kappa_y^e \frac{\partial}{\partial y} T_e \right)$$

$$= S_E^e - K (T_e - T_i) + \frac{1}{h_x} \left(u \frac{\partial}{\partial x} (n_e T_e) + v \frac{\partial}{\partial y} (n_e T_e) \right) \qquad (2.4)$$

Ion energy balance:

$$\frac{1}{\sqrt{g}} \frac{\partial}{\partial x} \left\{ \frac{\sqrt{g}}{h_x} \left(\frac{5}{2} n_i u T_i + \frac{1}{2} \rho u^3 \right) - \frac{\sqrt{g}}{h_x^2} \left(\kappa_x^i \frac{\partial}{\partial x} T_i + u \eta_x^i \frac{\partial}{\partial x} u \right) \right\}$$

$$+ \frac{1}{\sqrt{g}} \frac{\partial}{\partial y} \left\{ \frac{\sqrt{g}}{h_y} \left(\frac{5}{2} n_i v T_i + \frac{1}{2} \rho v u^2 \right) - \frac{\sqrt{g}}{h_y^2} \left(\kappa_y^i \frac{\partial}{\partial y} T_i + u \eta_y^i \frac{\partial}{\partial y} u \right) \right\}$$

$$= S_E^i + K (T_e - T_i) - \frac{1}{h_x} \left(u \frac{\partial}{\partial x} (n_e T_e) + v \frac{\partial}{\partial y} (n_e T_e) \right) \qquad (2.5)$$

Here the parallel transport coefficients are respectively η_x^i, κ_x^e and κ_x^i for viscosity and electron and ion thermal conductivity. Classical values are used for these and also for the coefficient K which describes equipartition. The corresponding transverse coefficients for radial transport are η_y^i, κ_y^e, κ_y^i and the diffusion coefficient D. These are taken to be anomalous with magnitudes comparable to present experiments, namely:

$\kappa_y^e/n_e = 2.0\ m^2/s$ $\qquad$ $D = 1\ m^2/s$

$\kappa_y^i/n_i = 0.2\ m^2/s$ $\qquad$ $\eta_y^i/\rho = 0.2\ m^2/s.$

Mass density is $\rho = m_i\ n_i$, the electron number density is $n_i = z_i n_i$ and the pressure $p = (n_e T_e + n_i T_i)$; for the deuterium-tritium plasma $z = 1$ and $m_i = 2.5\ m_{(proton)}$. The volume source terms are S_n, S_{mu}, S_E^e, and S_E^i and these refer respectively to particles, momentum and electron and ion energy. These sources arise from recycling at the target and chamber walls of the divertor and are derived from models of neutral particle transport.

Parameters $\sqrt{g}$, h_x and h_y are metric coefficients which allow the model to treat both scrape-off and divertor plasmas whose radial thickness and cross section vary with x. If h_y is a function of x, then the width of the scrape-off layer varies with x. If g varies with x then the flow experiences a change in area which can be related to the major radius of the plasma. This approach enables the model to treat a realistic scrape-off plasma geometry which, as can be seen in Figure 2.1, is thinest at the outer equitorial plane due to compression of the magnetic surfaces in the high β equilibrium conditions. The functional dependence of h_y is shown in Figure 2.2.

2.2 Application to NET

This paper reports the results of two-dimensional-modelling of plasma transport to both the inner and outer divertor targets of NET/INTOR. The scrape-off thickness ($h_y y$), which is shown in Figure 2.2, is in approximate accord with the contours of the equilibrium magnetic surfaces. The dimension x lies parallel to the magnetic field. Modelling starts at the surface (A → A') which lies within the main plasma at a distance - $0.25(h_y y)$ inboard of the separatrix; in this region any poloidal asymmetries which arise from divertor action are probably negligible so that the assumption of uniform input plasma conditions is likely to be valid. The input parameters at the surface (A → A') are:

Plasma power = 80 MW (66 transported by electrons, 14 by ions).

Plasma density n (adjusted so that n_{sx} at the separatrix is about

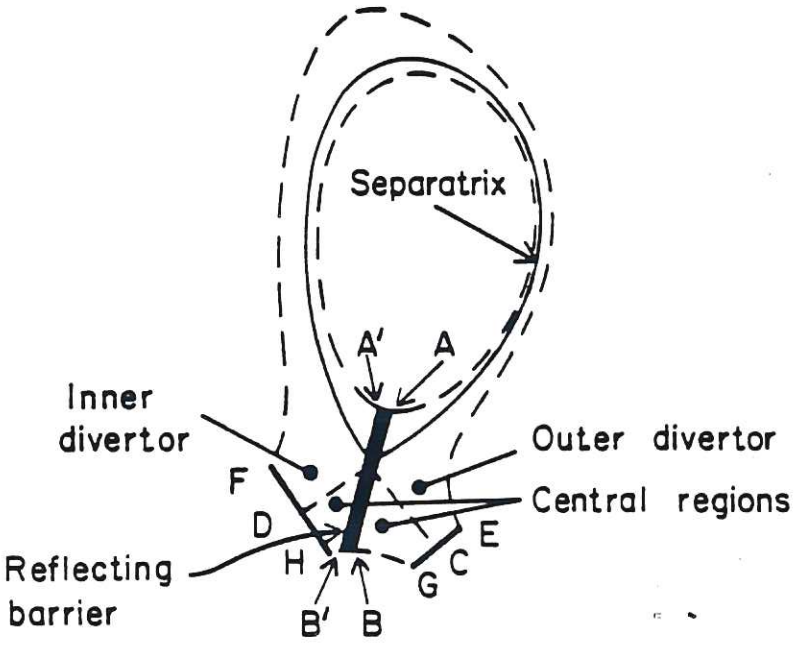

Fig. 2.1 The plasma region modelled (using the two-dimensional, fluid transport code) lies between the inner and outer dashed magnetic surfaces.
Note that modelling embraces regions which lie both inboard and outboard of the separatrix.

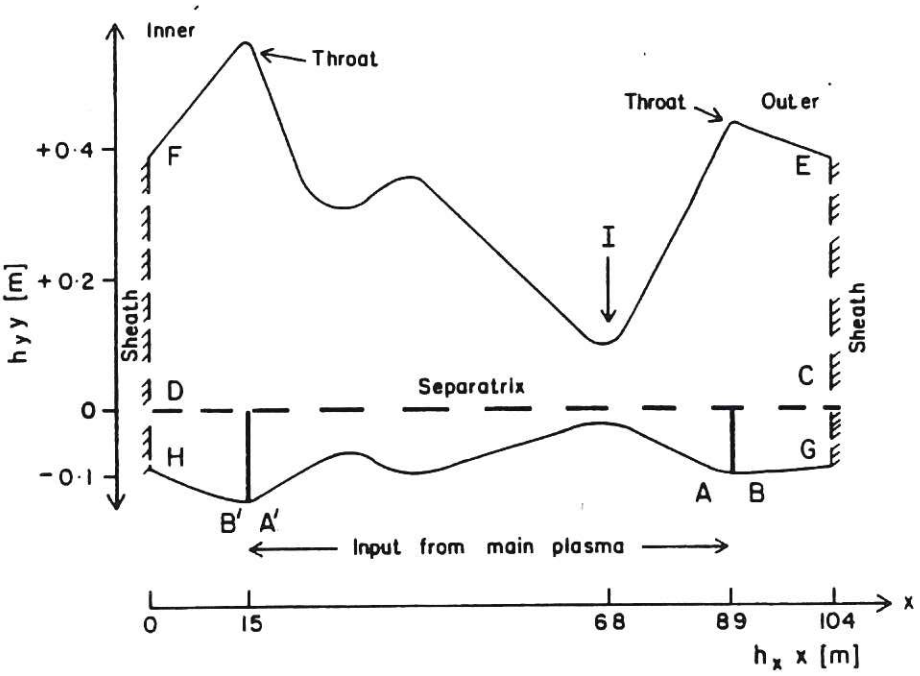

Fig. 2.2 Representation of the inner and outer divertor plasmas and the scrape-off plasma of INTOR.
The direction x lies parallel to the magnetic field.
Conditions used to bound the regions of fluid transport are described in the text.

$5 \times 10^{19}/m^3$).

Drift velocity $u = 0$.

The input flux of particles is not specified but it is adjusted by ascribing a recycling coefficient R^o at the outer divertor target so that the throughput of plasma ions corresponds to about 20 x (helium production rate), i.e. $\sim 10^{22}$ ions/s. The recycling coefficient at the inner target is set close to unity but it makes allowance for a flow of neutral particles from the inner to the outer plasma channels. A reflecting barrier (AA') is used to separate the outer and inner regions of the main plasma at the null-point and a similar barrier (BB') separates the outer and inner divertor plasma channels inboard of the separatrix. The conditions assumed for plasma reflection are:

$$u = 0;\ \partial n_i/\partial x = 0;\ \partial T_e/\partial x = 0 \text{ and } \partial T_i/\partial x = 0.$$

The separatrix intersects the outer and inner targets at C and D respectively and the corresponding radial extremities of the divertor plasma are E and F. Transport across the separatrix into the central region of the divertor is simulated by extending these central divertor plasma boundaries to G and H at the outer and inner targets respectively.

The boundaries of the fluid model which lie at $x = 0$ and $x = 104$ m are linked to a description of convective transport through the plasma sheaths at the divertor targets, namely:

$$\text{Parallel velocity; } u = \text{ion sound speed} = \sqrt{p/\rho} \qquad (2.6)$$

$$\text{Electron energy flux; } Q_x^e = \partial_e\, n_e u\, T_e \text{ [where } \partial_e = 4.8] \qquad (2.7)$$

$$\text{Ion energy flux; } Q_x^i = \partial_i\, n_e u\, T_i + \tfrac{1}{2}\rho u^3 \text{ [where } \partial_i = 2.5]. \qquad (2.8)$$

Radial transport to the first wall (surface E → F) and to the central region of the divertor [surfaces (B → G) and (B' → H)] is bounded by ascribing pedestal conditions at these surfaces; typical values are:

T_e and T_i in the range 2 to 4 eV; $\partial n_i/\partial y = 0$ and $\partial u/\partial y = 0$.

The power loading deposited upon the targets is determined by taking account of the particle energy reflection coefficient R_E of the target surface (in the present case tungsten). The release rate of sputtered target material is calculated but the influence of impurities on plasma transport and atomic power losses is neglected.

Source terms S_n, S_{mu}, S_E^e and S_E^i have, during this study, been determined by several simplified models of D/T recycling based upon the assumption that the only loss of particles is $\Gamma_\parallel^t(1-R^o)$ where $\Gamma_\parallel^t$ is the total ion flux to the outer divertor target. Typical examples of the distribution of atomic and molecular source terms throughout the xy mesh of the realistic divertor geometry have been determined using the NIMBUS Monte Carlo code and these have been used as a guide for developing the simpler models. The most recent model makes allowances for the attenuation by ionisation and by scattering (due to charge exchange) of atoms which move away from the target in the direction x. Motion in the direction y is simulated by weighting the profile of the atom flux $\Gamma_\parallel^t(y)$ in approximate accord to the effective mean free path for ionisation in the direction y (again taking account of scattering by charge exchange). Molecules are treated as atoms and no account is made of the energy transported to the target and walls by charge exchange atoms. Radiation losses from the atoms are accurately calculated. It is assumed that the momentum source term S_{mu} tends to zero because atom motion is predominantly transverse to the magnetic field.

At any mesh cell (x,y) the particle source is taken to be:

$$S_n(x,y) = R^o\Gamma^t \frac{n_e(x,y)\, S_i(x,y)\, \gamma(x,y)}{\Sigma\, n_e(x,y)\, S_i(x,y)\, \gamma(x,y)\, V(x,y)} \qquad (2.9)$$

where $V(x,y)$ is the volume of the cell, $S_i(x,y)$ the ionisation rate coefficient and $\gamma(x,y)$ is a dimensionless shape factor of the form:

$$\gamma(x,y) = \gamma_1(x,y) + \gamma_2(x,y). \qquad (2.10)$$

The component $\gamma_1(x,y)$ accounts for the range of the backscattered atoms and it is determined by numerical solution of

$$\frac{d}{dx}\gamma_1(x,y) = \lambda_{eff}^{-1}\, \gamma_1(x,y) \left[(B_{pol}/B_{tor}) \sin \alpha \right] \qquad (2.11)$$

where y is kept constant and $\gamma_1(x,y) = 1.0$ at the target. Here, λ_{eff} is the effective mean free path

$$\lambda_{eff}^{-1} = \lambda_i^{-1} + \lambda_{cx}^{-1} \qquad (2.12)$$

where λ_i and λ_{cx} are respectively the mean free paths for ionisation and charge exchange. The angle α is the inclination of the target to the magnetic surfaces. The second component accounts for the attenuation of thermal energy daughter atoms formed by charge exchange. Their effective penetration range is expressed as:

$$\lambda_{th}^{-1} = \left[\frac{8}{\pi}\frac{1}{\lambda_i}\left(\frac{1}{\lambda_i} + \frac{1}{\lambda_{cx}}\right)\right]_{th}^{1/2} \qquad (2.13)$$

and the component $\gamma_2(x,y)$ is determined by numerical solution of:

$$\frac{d}{dx}\gamma_2(x,y) = -\left[\lambda_{eff}^{-1}\right]_{th} \gamma_2(x,y)\left[(B_{pol}/B_{tor})\sin\alpha\right]$$

$$-\frac{1}{2}\frac{d}{dx}\gamma_1(x,y)\left[\lambda_i/(\lambda_i + \lambda_{cx})_{th}\right] \qquad (2.14)$$

where y is kept constant and $\gamma_2(x,y) = 0$ at the target.

2.3 Discussion of Predicted Plasma Conditions

The general properties of the scrape-off and the inner and outer divertor plasma channels are listed in Table 1. These results confirm that energy flow is predominantly concentrated in a thin scrape-off layer but, within the divertor, the peak of the plasma power density is reduced somewhat by transverse transport of energy across the separatrix into the central region of the divertor. High recycling conditions are readily established within the divertor and the peak plasma temperature does not exceed ~ 30 eV for typical operating conditions in NET/INTOR, i.e. 80 MW of plasma power distributed over the surface of the separatrix where the plasma density is $\sim 5 \times 10^{19}/m^3$. The two-dimensional calculations demonstrate that plasma power flows unequally to the inner and outer divertors, the power transported by the outer divertor channel being about 70% greater than that carried by the inner. The result arises from the poloidal asymmetry of the thickness of the scrape-off plasma and it is probably dependent upon the differing values of

TABLE 1 General properties of the scrape-off plasma and the inner and outer divertor plasma predicted for NET/INTOR

Parameter	Scrape-off	Targets	
		Outer	Inner
T_e (at separatrix)[eV]	136		
T_i (at separatrix)[eV]	200		
n_i (at separatrix)[$10^{19}/m^3$]	5.0		
Power deposited [MW]	0.9 first wall	42.3	23.4
Power radiated (by DT)[MW]		7.0	6.1
Ion flux to target [10^{24}/s]		4.0	4.1
Particle throughput [10^{21}/s] (recycling coefficients)	8.0	8.0 (R^o=0.998)	[21]* (R^o=0.995)
		* [Cross feed to outer divertor]	
Peak T_e [eV]		29.0	8.8
Peak T_i [eV]		10.9	6.6
Peak n_i [$10^{20}/m^3$]		2.4	6.1
Peak power flux density (in plasma ∥ to magnetic field) [MW/m^2]		196 (electrons) 65 (ions)	99 (electrons) 57 (ions)
B_{pol}/B_{tor}		1/11.25	1/11.25
Peak power load on target [MW/m^2 ⊥ to magnetic surfaces]		19.1	12.3
Scale-length of load (full width at half height ⊥ to magnetic surfaces)[10^{-2} m]		4.2	4.0
Rate of sputtering [D/T ions]		Negligible	Negligible

TABLE 1 (continued)

Parameter	Scrape-off	Targets	
		Outer	Inner
Rate of sputtering* by He^{2+} (10^{19} W atoms/s) *[1.1% of ion flux to target - see Section 3.3]		1.2	Negligible
Peak erosion [mm of W/y] (100% availability)		9	Negligible

Prescribed input power = 80 MW (66 MW by electrons, 14 MW by ions)

Prescribed radial transport coefficients; κ_y^e/n_e = 2 m^2/s and D = 1 m^2/s

electron temperature and hence parallel thermal conductivity ($\kappa_x^e T_e^{5/2}$) adjacent to the fluid boundaries at the inner and outer targets. The model makes no allowance for any poloidal variation in κ_y^e.

Peak power loading at the outer target is sufficiently high (~ 19 MW perpendicular to the magnetic surfaces) to require that the target be inclined to the magnetic surfaces. When the inclination is 15^o (assumed also in the Monte Carlo calculations discussed in Section 3) the peak load is reduced to about 5 MW/m^2 which is compatible with engineering constraints. The lower loading at the inner target (~ 12.5 MW/m^2 perpendicular to the magnetic surfaces) can be accommodated upon a horizontal target.

Plasma temperature adjacent to the targets is so low that very few of the incident D/T ions have energies in excess of the sputtering threshold of tungsten. Release of tungsten due to D/T ion sputtering is therefore negligibly small. The source of tungsten impurities is due to the small component of He^{2+} ions incident upon the target. Smaller contributions may arise from oxygen and iron ions which enter the divertor from the scrape-off plasma. A realistic upper estimate of the sputtering rate appears to be $\Gamma_w^o \sim 1.2 \times 10^{19}$ W atoms/s and the fraction of these impurities which must be retained within the divertor can be crudely expressed as:

$$\xi = 1 - \left(\frac{C\langle n\rangle V}{\Gamma_w^o \tau}\right) \qquad (2.15)$$

where $C = 10^{-4}$ is the acceptable concentration of tungsten ions within the main plasma where the average density is $\langle n\rangle \sim 1.4 \times 10^{20}/m^3$ and the volume is $V \sim 240\ m^3$. If the impurity containment time, τ, is conservatively assumed to be 5s then a retention efficiency of not less than 94% is required. This retention relates to the combined action of the divertor and the screening effect of the scrape-off plasma so that the requirement appears to be realistic. These results therefore confirm the selection of tungsten as an appropriate target material for NET/INTOR.

2.4 Asymmetries within the Scrape-off Plasma

Previous modelling for INTOR and NET has hitherto included the

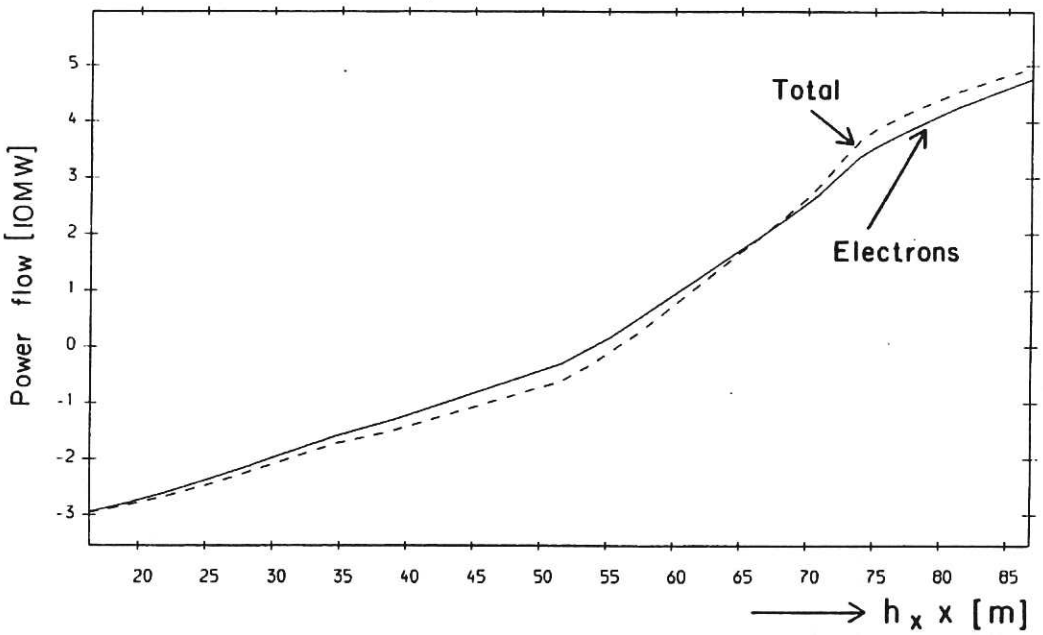

Fig. 2.3 Power flow in the scrape-off plasma plotted as a function of the distance h_x x along the magnetic field.
The solid curve shows power transported by electrons only and the dashed curve shows the total power flow.
Positive flow is towards the outer divertor.

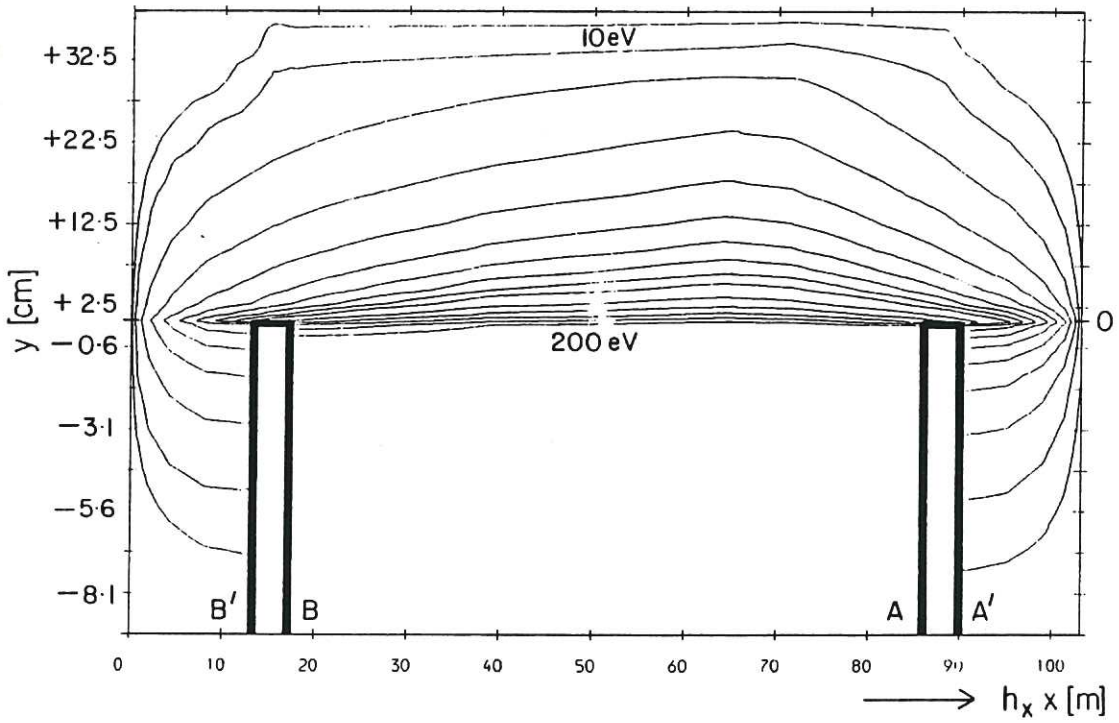

Fig. 2.4 Isotherms of ion temperature
Increments of temperature are 10eV below 100eV and 20eV above 100eV.

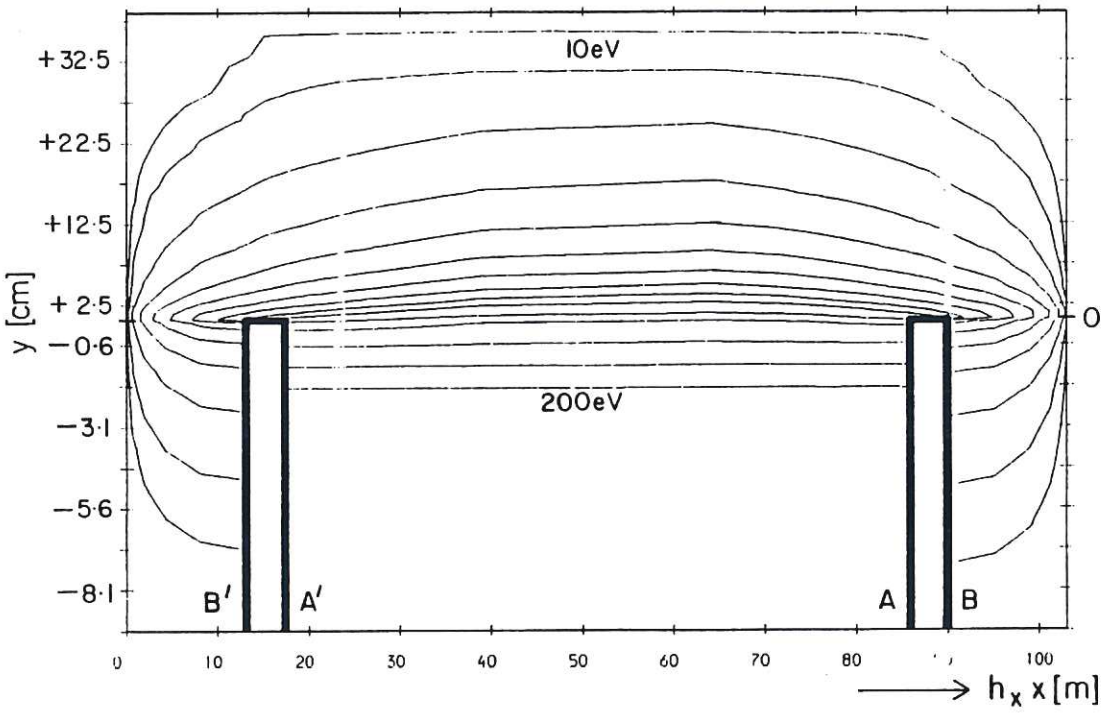

Fig. 2.5 Isotherms of electron temperature.
Increments of temperature are as in Fig. 2.4.

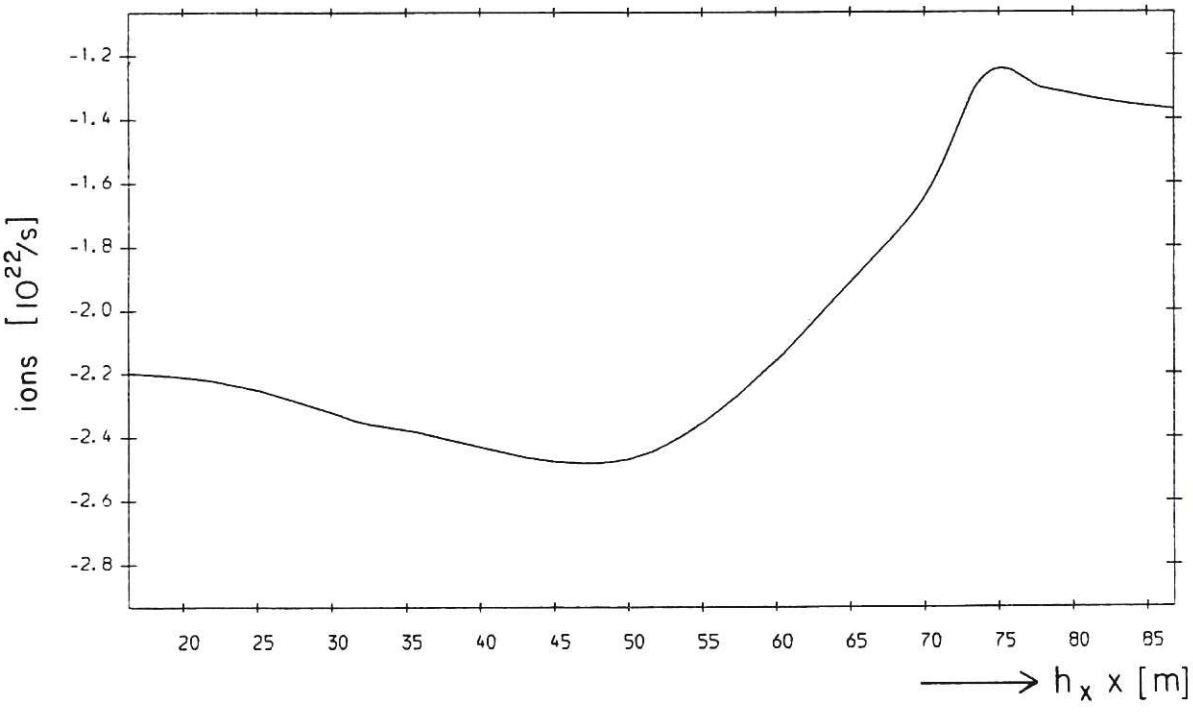

Fig. 2.6 Particle flow along the scrape-off plasma.
Negative flow is towards the inner target.
Note that the flow is unidirectional and arises because of the coupling, by neutral particles, of the inner to the outer divertor channels.

assumption that the plasma power is distributed equally to the inner and outer divertors. Results of the present more sophisticated treatment are shown in Figure 2.3 and indicate that transport of energy by electrons within the scrape-off plasma changes its direction at about the mid-length of the magnetic flux tubes which link the inner and outer targets. However the power fed to the outer divertor channel is about 1.7 times that to the outer. The isotherms of T_i, shown in Figure 2.4, display an asymmetry which correlates rather well with the location of the thinnest region of the scrape-off plasma. In contrast, the isotherms of T_e, shown in Figure 2.5, tend to be symmetrical because of the more powerful clamping of electron temperature by conduction along the magnetic field.

A tentative explanation of this behaviour is as follows; when plasma transport is being first established in the scrape-off layer there is an initial tendency for energy to be equally distributed to the inner and outer divertors but the effective connection length for particle transport is unequal because of the asymmetry in thickness of the scrape-off. The length to the inner divertor is greater than to the outer. Thus the energy associated with each transported particle is less at the inner divertor and hence the plasma temperature is lower. Due to the strong temperature dependence of the parallel electron thermal conductivity there rapidly becomes established an asymmetry in energy losses from the opposite ends of the flux tubes linking the divertor targets. Once established, this inequality is retained even in steady state conditions when the particle flow to the throats is substantially reduced. To avoid overestimating this asymmetry a fraction (5×10^{-3}) of the neutral particles released at the inner target is allowed to flow into the outer divertor plasma. (This is in accord with Monte Carlo calculations for the realistic divertor geometry described in Section 3.2). The plasma model does not take consistent account of charged particle transport between the inner and outer channels within the divertor chamber, but plasma conditions at the opposite faces of the artificial barrier BB' (which separates the inner and outer regions shown in Figures 2.1 and 2.2) are found to be comparable. This fact indicates that the assumption of plasma reflection at the barrier provides a reasonable allowance for plasma coupling.

The rate at which neutrals are allowed to flow from the inner to outer divertor channels is taken to be greater than the rate at which

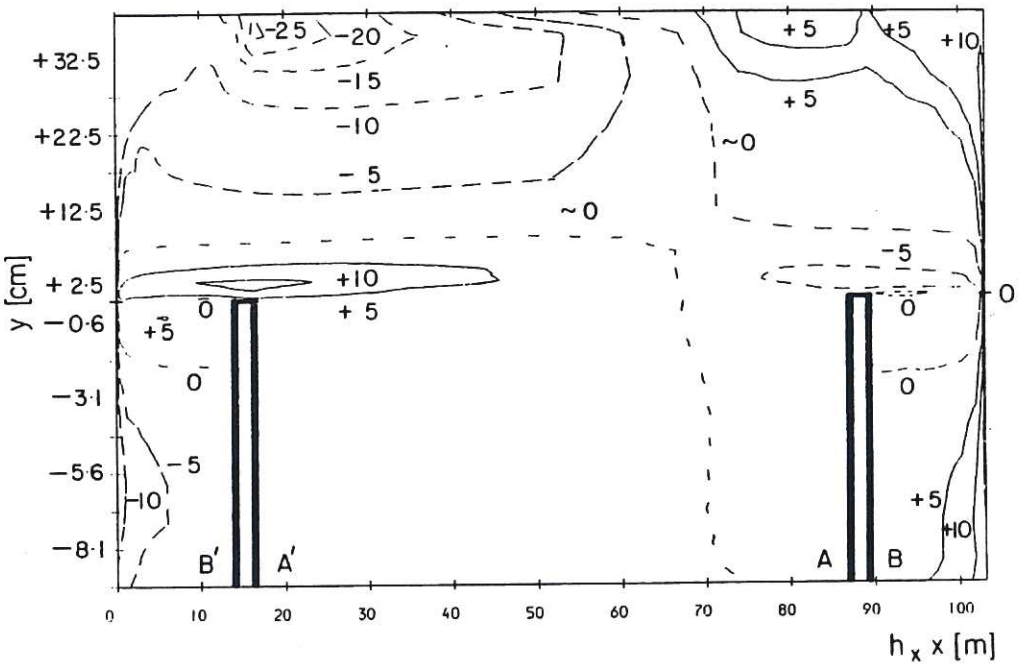

Fig. 2.7 Contours of parallel flow velocity in both the scrape-off and divertor regions.
Solid lines show "positive" flow towards the outer target and dashed lines "negative" flow towards the inner (units are 10^3 m/s).
Note that, the flow reverses around the separatrix adjacent to both of the divertor entrances.

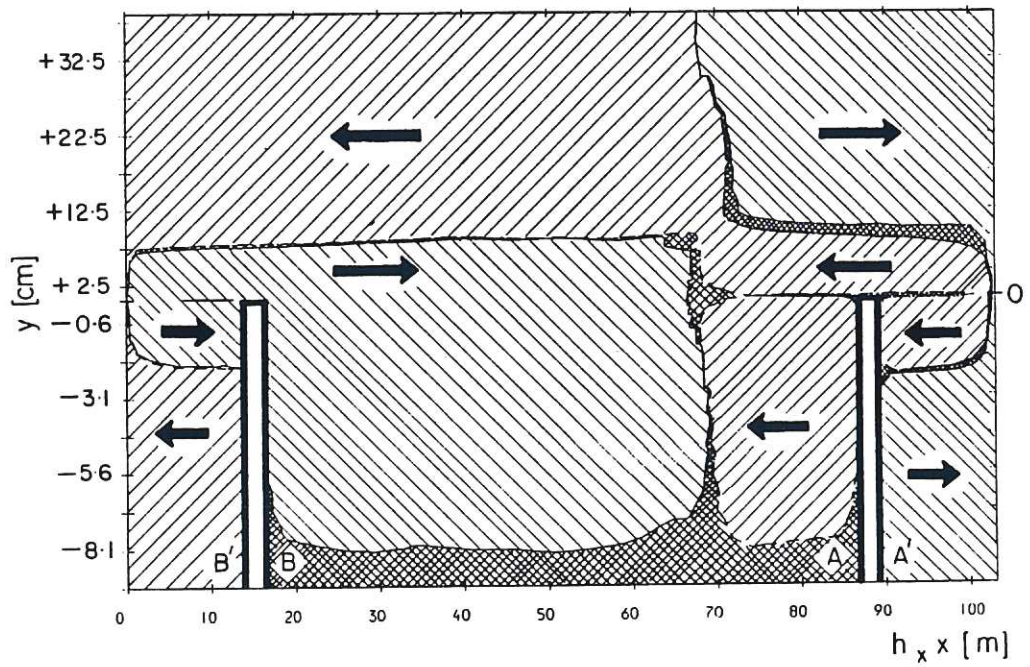

Fig. 2.8 Two-dimensional plot of the helium ion entrainment criterion of Neuhauser et al.[10].
Cross hatching shows regions where the entrainment criterion is violated.
Arrows show direction of entrained flow.

D/T gas is pumped from the outer divertor. This sets up a net circulation of plasma particles which, as can be seen in Figure 2.6, flow from the scrape-off into the inner channel and return via the outer divertor channel to the scrape-off plasma.

2.5 Impurity Transport

Even though the net particle flow has a preferred direction within the scrape-off there are regions where the local flow velocity is reversed. The steady state, two dimensional distribution of flow velocity, u, parallel to the magnetic field can be seen in Figure 2.7. The model indicates that there is some backflow of plasma particles into the scrape-off through the divertor throats and also into the main plasma close to the separatrix. This backflow extends to the thin asymmetric region of the scrape-off plasma. The consequent circulation of plasma in the divertor throats may degrade somewhat the retention and exhaust of impurities. Neuhauser et al.[10] have considered the balance between the frictional forces which entrain impurity ions within the drifting boundary plasma and the opposite tendency for these impurities to thermally diffuse along the magnetic field towards regions of higher ion temperature. They have identified a criterion, $M \geq \lambda_i/\lambda_T$, which when satisfied implies that highly charged impurities tend to be entrained and thereby drift with the background plasma. Here M is the Mach number of the drifting plasma, λ_i the Coulomb collision mean free path (for D/T ions - impurity ions) and λ_T the scale length of the D/T ion temperature. Evaluation of the present data, illustrated by Figure 2.8, shows that the criterion is satisfied close to the divertor targets where D/T recycling causes the Mach number to be high. Thus sputtered target atoms should readily be recycled to the target. It is also satisfied in the outermost layer of the scrape-off and divertor channels except for a relatively small region at the thinnest part of the scrape-off where $|u| \to 0$. On either side of here the velocity u is unidirectional and directed towards the divertor target. This layer extends inwards for about half of the scrape-off thickness and it is sufficiently dense and thick to ensure that any low-energy impurity atoms released from the first wall will be ionised within the layer. Exhaust of wall impurities into the divertor chamber is thus unlikely to be substantially degraded by thermal diffusion. Inboard of this layer, and more particularly towards the separatrix, the entrainment criterion is violated and

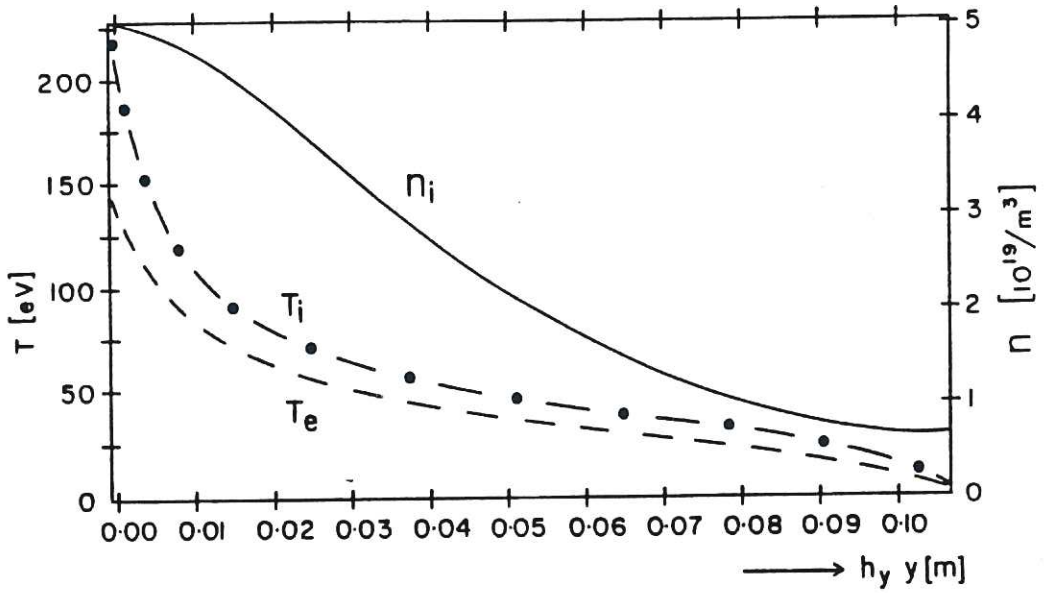

Fig. 2.9 Radial profiles of T_e, T_i and n_i at the narrowest region of the scrape-off plasma.
Location along the magnetic field is shown by I in Fig. 2.2.

moreover there are regions where the flow velocity is directed outwards from the divertor towards the scrape-off. Helium ions from the central plasma must first flow across the separatrix and traverse this inner layer of complex flow patterns before being exhausted as gas from the divertor. It is therefore probable that helium exhaust from the inner layer may be substantially degraded. This is much less likely to pertain in the outer layer which is in fact linked to about 20% of the particles which recycle to the divertor target. It would therefore be prudent to enhance the vacuum pumping speed in order to lower the helium concentration within the outer layer (say to ~ 2%) and thereby avoid an unacceptable concentration in the vicinity of the separatrix.

2.6 The First Wall

Radial profiles of T_e, T_i and n_i within the scrape-off at its thinnest region (i.e. at I in Figure 2.2) are shown in Figure 2.9. The values at the separatrix, $T_e \sim 136$ eV, $T_i \sim 200$ eV and $n_i \sim 5.0 \times 10^{19}/m^3$ do not differ substantially from those previous predicted for the scrape-off[7]. Goedheer has used a somewhat comparable temperature profile to predict the velocity distribution of charge exchange atoms formed by recycling at the first wall[11]. His model, which is based upon a solution of the Boltzman equation coupled to a one-dimensional, steady state code for radial plasma diffusion, predicts that the charge exchange flux to the first wall should be 4.7×10^{20} hydrogen atoms/m^2/s in order that a plasma density of $\sim 4 \times 10^{19}/m^3$ can be maintained at the separatrix. About 5% of the atoms incident upon the first wall then have velocities in excess of 40 eV and 5% in excess of 100 eV. Taking 250 eV as a reasonable average energy of the faster group and allowing for a 50% concentration of tritium atoms indicates that the sputter rate of a stainless steel wall is $\sim 3.3 \times 10^{17}$ Fe atoms/m^2/s and the erosion rate (neglecting redeposition) is ~ 0.1 mm/y (100% availability). This sputtering pertains only to the outer periphery of the plasma (where the scrape-off is ~ 10 cm thick), it will be significantly reduced at the inner periphery where the scrape-off layer is thicker. A screening efficiency of about 90% is required in the edge plasma to ensure that the central iron concentration does not exceed 10^{-3} (the assumed impurity containment time being 5s).

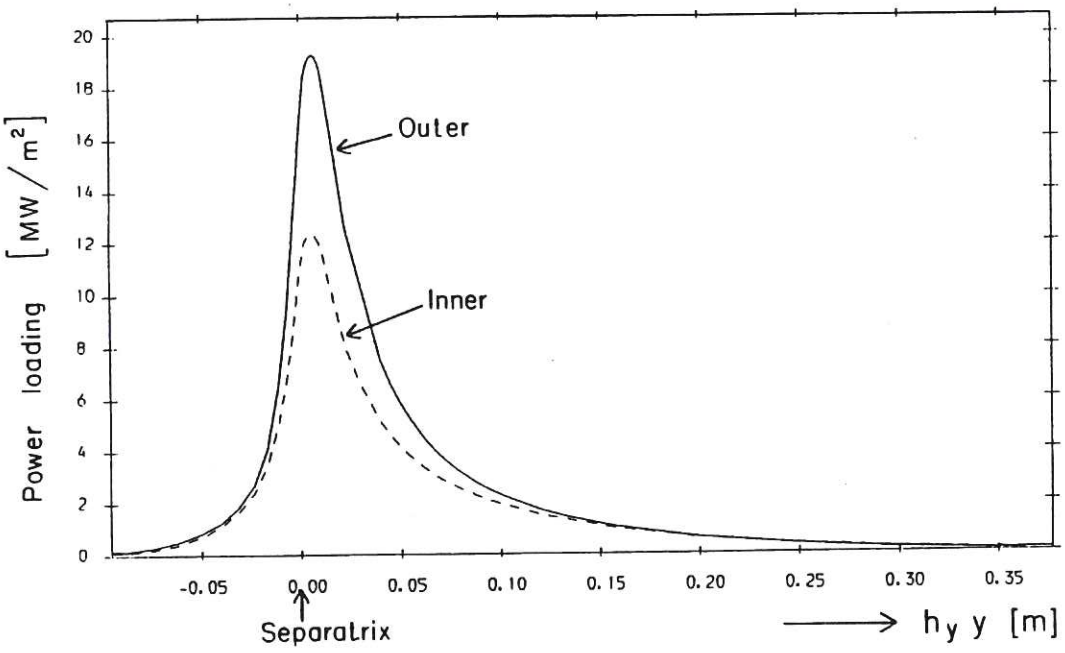

Fig. 2.10 Radial profiles of the power load deposited upon the tungsten targets.
The dimension $h_y y$ lies perpendicular to the magnetic surfaces.
The solid curve refers to the outer target and the dashed curve to the inner.

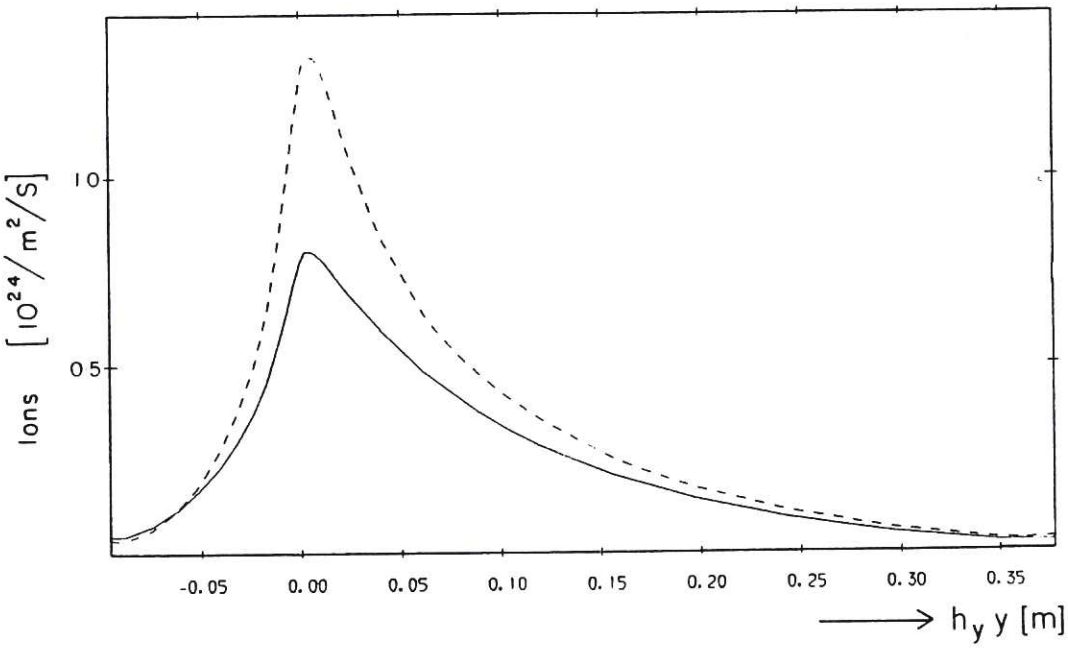

Fig. 2.11 Radial profiles of the particle flux density at the targets.

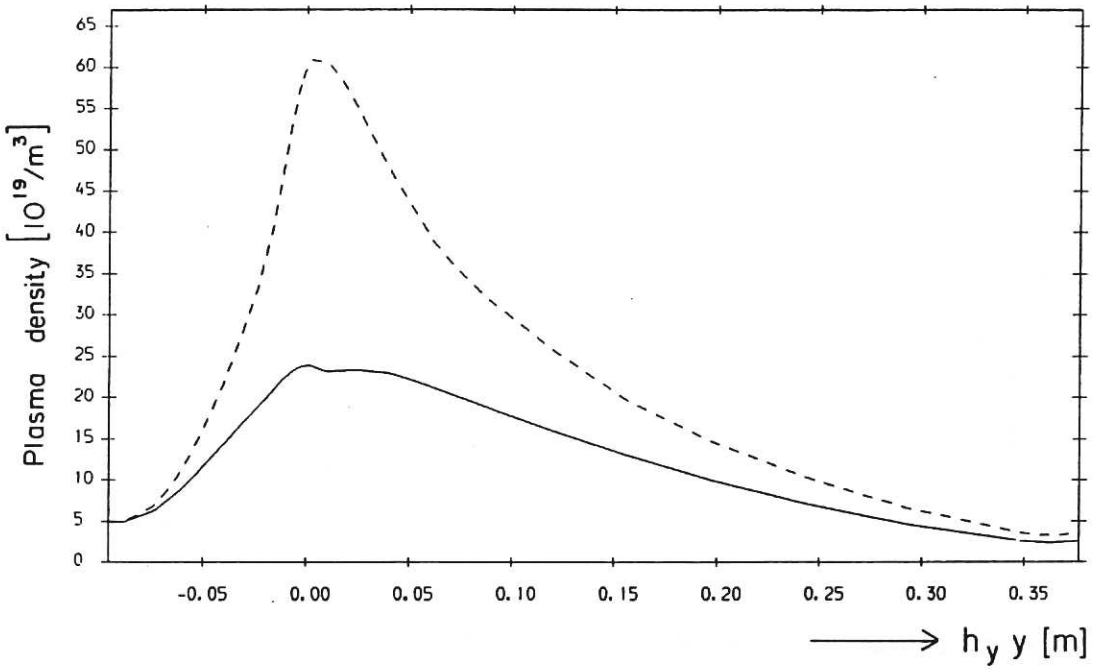

Fig. 2.12 Radial profiles of n_i at the outer and inner divertor targets.

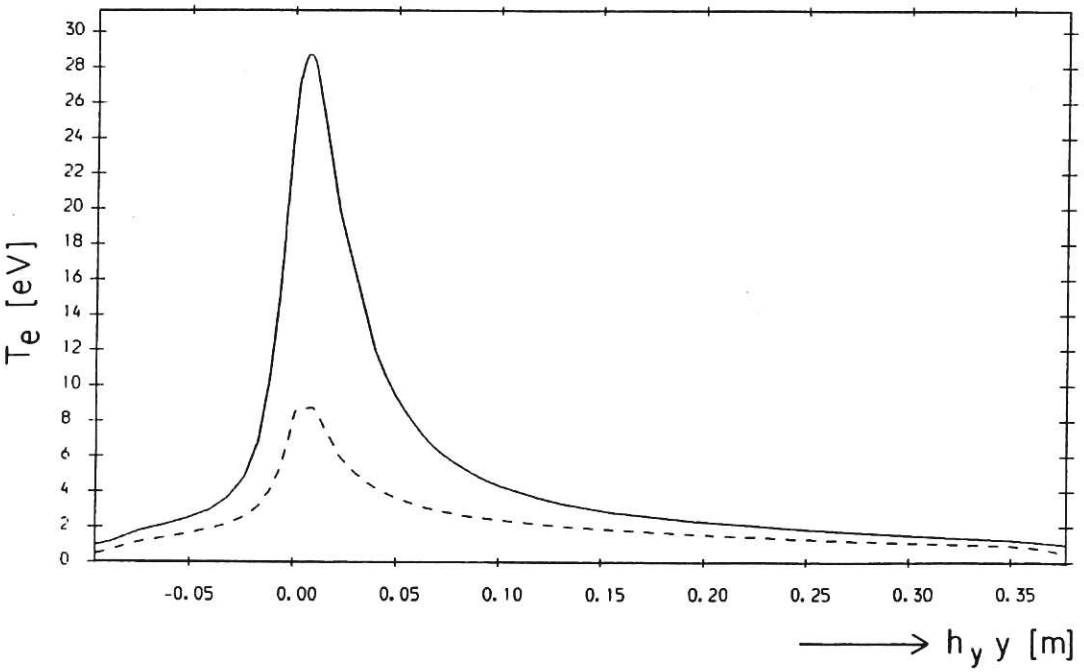

Fig. 2.13 Radial profiles of T_e at the divertor targets.

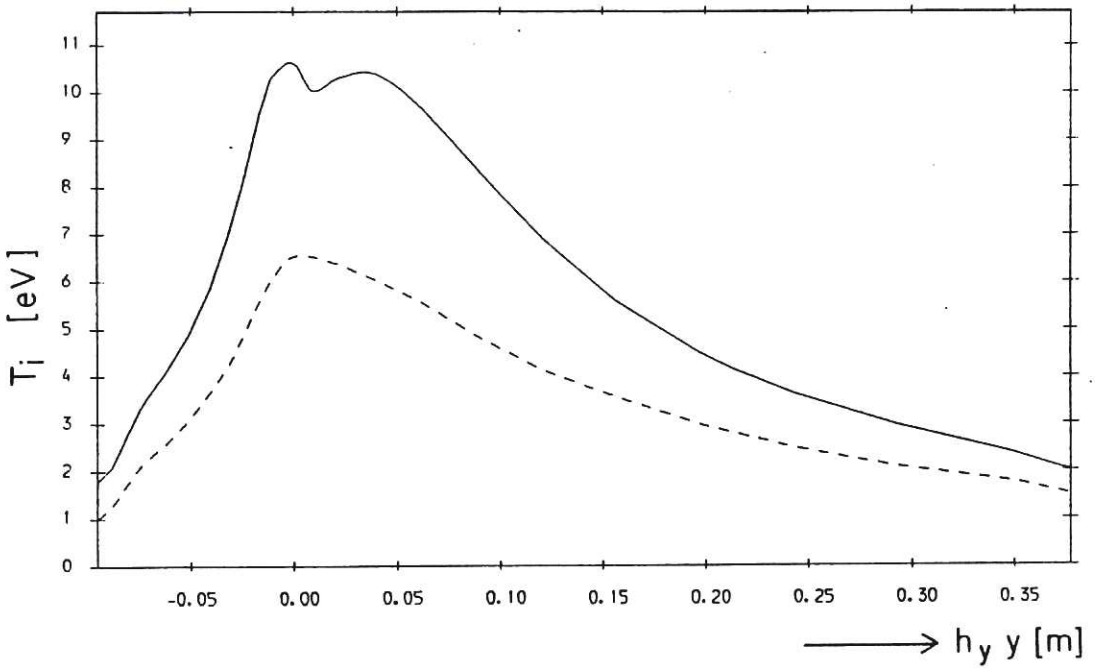

Fig. 2.14 Radial profiles of T_i at the divertor targets.

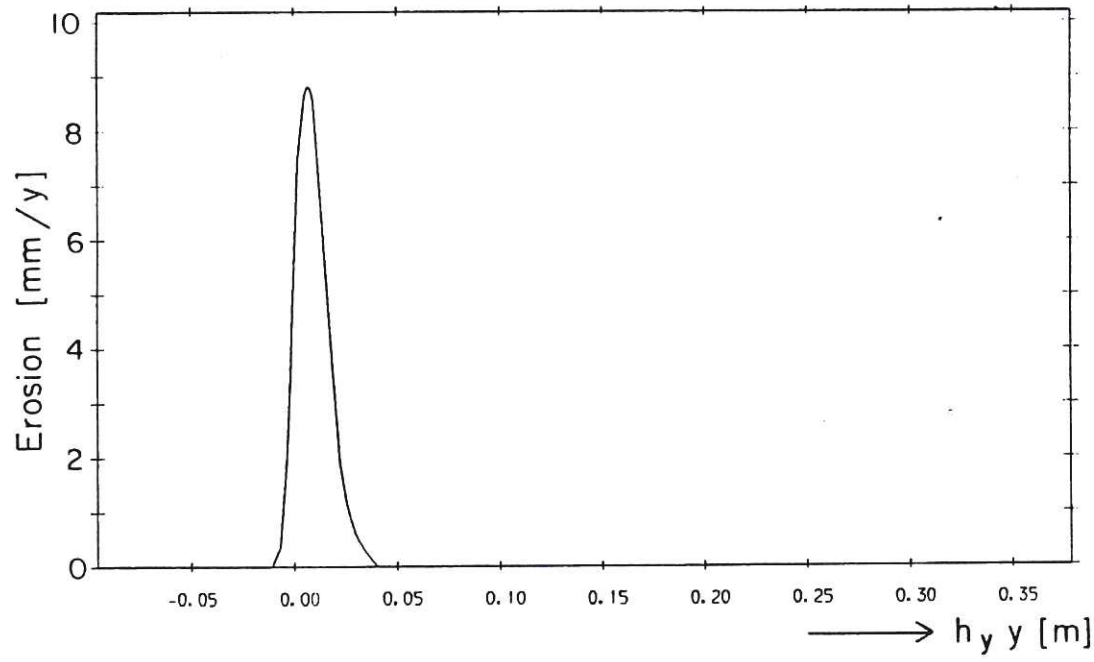

Fig. 2.15 Profile of erosion depth due to sputtering of the outer tungsten target.
Redeposition is neglected.
Note that erosion is reduced by a factor (sin α) where α is the angle at which the target is inclined to the magnetic surfaces.

2.7 Conditions at the Divertor Target

Peak values of the plasma parameters are listed in Table 1. The power load deposited upon the targets due to the kinetic energy of the plasma ions (with due allowance for backscattering) plus the 13.6 eV potential energy of these ions is plotted as a function of h_{yY} (namely the distance perpendicular to the magnetic surfaces) in Figure 2.10. These radial profiles are narrow (~ 4.5 cm full width - half height) and are similarly shaped at both the outer and inner targets. Profiles of particle flux density are shown in Figure 2.11, these are broader, about 20 cm and 13 cm (FW-HH) respectively at the inner and outer targets. The density profiles are shown in Figure 2.12. They are somewhat broader still. The electron temperature profiles presented in Figure 2.13 are narrow (~ 5cm, FW-HH) and similarly shaped at the inner and outer targets whereas the ion temperature profiles shown in Figure 2.14 are much broader.

When redeposition is neglected, the erosion depth profile for sputtering of the outer tungsten target by D^+, T^+ and (1.1%)He^{2+} is as shown in Figure 2.15. The half width - half height is only ~ 2 cm which for a target inclined at 15^o corresponds to ~ 7 cm. Peak erosion in the direction y is ~ 9 mm/y (100% availability) which corresponds to about 2 mm/y on the inclined target. There is negligible sputtering of the inner target.

Estimation of the true erosion rate is uncertain because the ion energies lie close to the sputtering threshold and also the displacement (in the y direction) of redeposited material could have a significant effect upon such narrow profiles. Moreover, uncontrolled motion of the plasma channel probably exceeds the width of the erosion profile. The location of the null-point can at best be controlled to $\pm$ 1 cm which implies that plasma-location at the outer target (inclined at 15^o) is uncertain to at least 4.7 and 6.1 cm due to movement of the null-point in the vertical and horizontal directions respectively. Uncontrolled motion of the plasma within these limits might influence erosion to a greater extent than the uncertainties of plasma modelling. If the position control system of the plasma can be so operated that the divertor plasma is continuously scanned over the target then the erosion depth would be considerably reduced and, moreover, present uncertainties in the spatial characteristics of redeposition can probably be ignored.

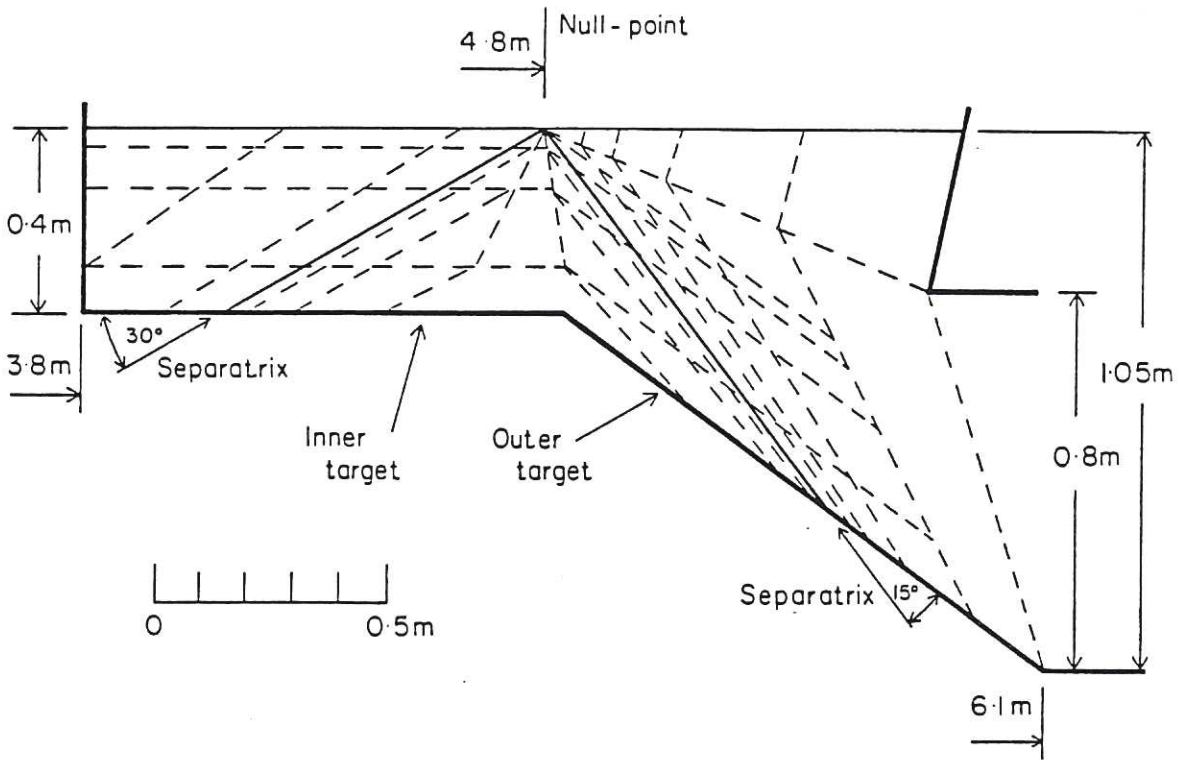

Fig. 3.1 Two-dimensional diagram of the "short" divertor chamber of INTOR used in the present study.
The separatrix surfaces are indicated by solid lines which are inclined at 15^{o} and 30^{o} to the outer and inner targets respectively. Dashed lines show the mesh employed in the Monte Carlo calculations.

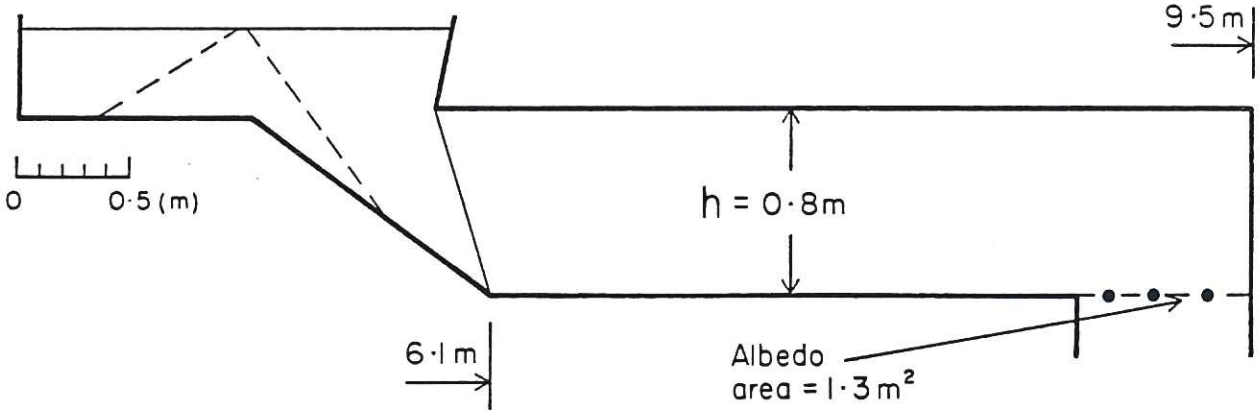

Fig. 3.2 Two-dimensional diagram of the chamber and pumping duct used in the model.
The entrance area of the downpipe is assumed to be $1.13\,m^2$ and the albedo is adjusted so that the exhaust of helium atoms through 12 downpipes is 2×10^{20} He atoms/s.

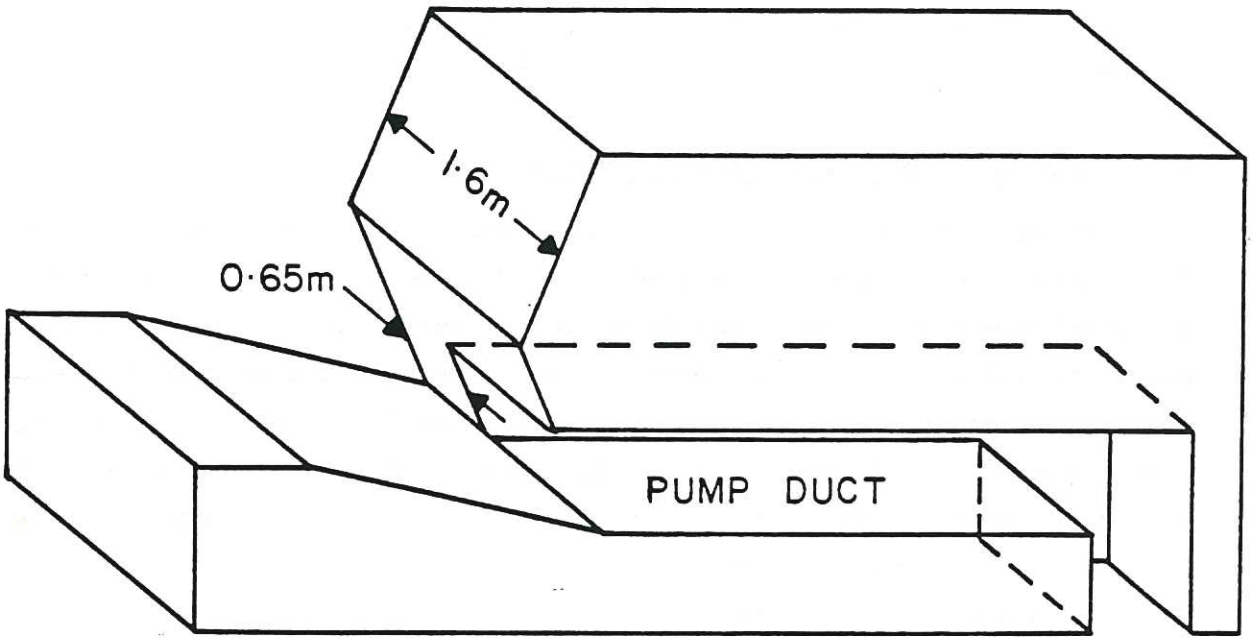

Fig. 3.3 A perspective view of the geometry of the outer chamber and duct used in the model.
The width of each pumping duct is assumed to be 1.9 m.

3. MODELLING OF NEUTRAL PARTICLE TRANSPORT

The three-dimensional Monte Carlo code NIMBUS is applied within the geometry of the inner and outer channels of the single-null poloidal divertor chamber and the pumping duct. This treatment is used to calculate sources or sinks of particles, momentum and energy arising from the recycling of D/T neutral particles. It is also used to determine the spatial distribution of erosion and redeposition of wall material sputtered by neutral particles as well as the power loading on the chamber walls. In addition, particle retention within the chamber and the pumping speed necessary to exhaust helium are calculated. The numerical method together with the surface and atomic processes included in NIMBUS are described by Cupini et al[12].

3.1 Application to the NET/INTOR Divertor

The geometry of the divertor chamber and the mesh used in the Monte Carlo treatment are shown in Figure 3.1. This configuration is in fact a "short" divertor chamber insofar as the target surface lies only 0.4 m below the null-point. It is adopted firstly because the predicted power load on the outer target is such that an inclination of about 15^{o} to the magnetic surfaces is required in order to make the peak load approach the engineering criterion of 5 MW/m^2. Secondly it is necessary to restrict the chamber depth to about 1 m below the null-point in order to accommodate it within the toroidal field coils. The peak power load to the inner target is less by about a factor two so that there is little need to incline the inner target below the horizontal plane, which corresponds to an inclination of about 30^{o} to the magnetic surfaces.

The Monte Carlo treatment extends throughout the horizontal region of the pumping duct and terminates at the entrance to the downpipe which feeds the vacuum pump. The conductance of the downpipe plus vacuum pump is represented by an albedo region whose area realistically represents the entrance of the downpipe. The two-dimensional geometry of the chamber and pumping duct is shown in Figure 3.2. The calculation takes full account of the 12 pumping ducts envisaged for INTOR, but the 16 duct system envisaged for NET has not yet been analysed. The three-dimensional properties of the duct and outer wall of the divertor chamber are sketched in Figure 3.3.

The distribution of plasma parameters throughout the mesh used in

NIMBUS is taken from the two-dimensional plasma model in which a simple treatment of recycling (described in Section 2.2) is used to provide initial source terms. More precise source terms arising from both atoms and molecules of D/T are derived from the Monte Carlo treatment; these account for dissociation of molecules, ionisation and excitation of both atoms and molecules and also charge exchange between D/T atoms and ions. Transport of neutral helium is simulated by introducing a small amount of helium into the flux of neutral particles released from the target. The concentration of helium atoms at the target (about 1.1%) corresponds to a concentration of 5% of He^{2+} ions in the D/T plasma at the divertor throat. It is determined using the following assumptions

(a) Helium ions drift with the same velocity as the background D/T plasma.

(b) The radial profile of helium ion density is the same as that of the background D/T plasma.

(c) The presence of He^{2+} does not influence the properties of the D/T plasma predicted by fluid modelling.

(d) Helium ions enter the plasma sheath as He^{2+}.

(e) Helium atoms comprise 5% of the total number of neutral particles pumped

and

(f) The vacuum pumps have equal volumetric capacity for D/T and helium.

The pumping speed of each of the 12 downpipes plus their vacuum pumps is determined by adjusting the albedo at the entrance area of each pipe (1.13 m^2) so that a total of 2×10^{20} He atoms/s are pumped. The speed of the vacuum pump which must be located at the extremity of the downpipe is of course dependent upon the conductance of the pipe.

The materials selected for the present study are tungsten for the target surface and stainless steel for the chamber walls and pumping ducts. Particle surface interactions are treated as described in

Ion flux to targets [10^{24}/s]	4.0 (outer)	4.1 (inner)
Concentration of He^{2+} at target [%]	1.1	
Concentration of helium in pumped gas [%]	5	
	DT	Helium
Pumping rate of neutrals [10^{20}/s]	40	2.0
Albedo	0.954	
Area of each downpipe	1.13 m^2	
Equivalent pumping speed of each downpipe plus pump [m^3/s for He at 300 k]	14.5	
Total pumping requirement [m^3/s]	174	
Fraction of He^{2+} ion flux to outer target which is pumped as neutrals	0.46 x 10^{-2}	
Fraction of total ion flux to inner target which is pumped as neutrals	$<<10^{-4}$	
Probability for escape into main plasma [%]	0.35	16
Average energy of escaping neutrals [eV]	34	40
Probability of D/T cross feed to outer divertor	0.25 x 10^{-2}	
Probability of D/T cross feed to inner divertor	negligible	
Power deposited upon chamber walls by neutrals [MW]	1.1	
Power flow into downpipe [W]	400	
Release rate of stainless steel from walls due to sputtering of neutrals [10^{20}/s]	0.82	7.6

TABLE 2 General behaviour of neutral particle transport within the single-null poloidal divertor and pumping ducts of NET/INTOR.

Ref. 12 with the exception that particle reflection coefficients recently calculated by Eckstein[13] are used for low energy D/T particles.

3.2 Recycling and Erosion

The general behaviour of neutral particle transport within the divertor chamber and pumping ducts is listed in Table 2. It is evident that the inner target contributes negligibly to gas exhaust but this is not important because only about 0.5% of the helium ions incident upon outer target need be pumped. The total pumping requirement predicted for the 12 downpipes (including vacuum pumps) is about 175 m^3/s for helium atoms at 300K. The concentration of helium in the pumped gas is enriched by a factor 4.6 relative to the helium concentration at the outer target.

Despite the "shortness" of the divertor chamber, high recycling conditions are readily attained because only 4×10^{-3} of the total flux of D/T plasma ions incident upon the inner and outer targets return as neutrals to the scrape-off and main plasma. The relatively small number of D/T particles which escape is unlikely to enhance the charge exchange atom flux to the first wall in the vicinity of the divertor throat. The analysis shows that between 0.25 to 0.5% of D/T particles formed at the inner target escape into the outer divertor channel. There is negligible flow in the reverse direction, probably due to the inclination of the outer target which tends to direct neutrals towards the outer wall of the chamber.

The divertor is less effective in retaining helium, about 16% of the He^{2+} ions incident upon the target return to the scrape-off and main plasma as helium atoms with an average energy of 40 eV. This is due (a) to the relatively high energy of backscattered helium atoms, (b) to their small ionisation cross section and (c) to the virtual absence of helium atom scattering due to charge exchange collisions. This backflow of helium atoms has not yet been consistently treated in the Monte Carlo code nor has its influence upon helium ion transport been assessed.

The total power load deposited upon the chamber walls by neutral particles is only about 1.1 MW. The power flow into the downpipes is only 400 W so that the gas entering the pumps is likely to be sufficiently cold to guarantee effective pumping action.

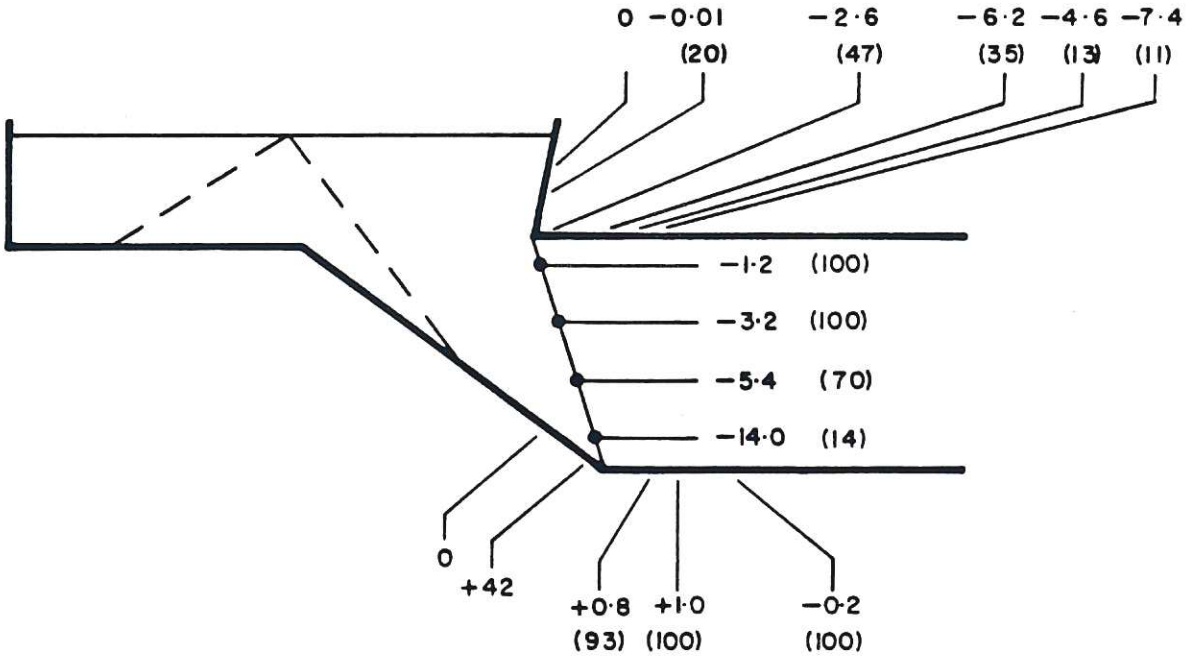

Fig.3.4 Spatial distribution of the net erosion of the chamber walls and pumping duct.
Net erosion is -ve and net deposition +ve; the units are mm/y (100% availability).
The percentage of the effect due to helium atoms is shown by the bracketed values.

The total release rate of iron atoms sputtered from the chamber walls is 8 x 10^{20}/s and the spatial distribution of the net erosion arising from the balance between sputtering and redeposition is shown in Figure 3.4. Also shown (in brackets) is the fraction of net erosion due to helium. The greatest erosion (about 14mm/y for 100% availability) occurs at the lower region of the chamber wall in between the pumping ducts. This relatively powerful sputtering is due largely to DT particles. Sputtering decreases as the spacing between the target and the wall is increased but the fraction arising from helium then increases doubtless due to the greater ability of the relatively energetic helium atoms to escape from the thicker regions of the divertor plasma. Erosion of the pumping duct occurs along its upper surface whereas there is a net deposition upon the lower surface.

The Monte Carlo treatment deals accurately with redeposition of sputtered atoms which do not enter the plasma. A simple concept of ion transport along the field to the target is introduced in those cases where wall material enters the plasma and is subsequently ionised. This treatment shows that there is a substantial redeposition of iron upon the outer periphery of the divertor target but this does not extend inwards further than one mesh cell of the model (i.e. 0.18 m). The deposition rate, neglecting re-sputtering which is unlikely in this cold extremity of the plasma, is about 42mm/y. The wall erosion and build-up on the target could be reduced by several orders of magnitude if tungsten armour were suitably deployed on the chamber wall.

3.3 Optimisation of Geometry

Earlier studies [9] have shown that the optimum pumping performance is attained when the height h (see Figure 3.2) of the pumping duct does not exceed ~ 50 cm. This study was based on less consistent plasma data but preliminary checks using the present two-dimensional plasma data confirm that the optimum height is likely to be 0.2 to 0.3 m. It seems to be unimportant whether the duct is of uniform height, is restricted in height only at its entrance, or is tapered towards its entrance. The implication is that the results reported here (based on a uniform height of 0.8 m) overestimate the pumping requirements by about a factor two.

4. VALIDITY AND REACTOR RELEVANCE OF MODELS

Two dimensional plasma modelling has reinforced the view that the open throated, single-null divertor will operate in a high recycling regime and, if the target surface is tungsten, then the divertor also provides a very credible concept for control of plasma composition. There are of course a number of uncertainties inherent in fluid modelling and although present experimental evidence supports the general patterns of predicted behaviour the breadth of data is insufficient to provide detailed validation. On the other hand, there are aspects of reactor engineering and methods of operation which may in practice override some of the present uncetainties in modelling. It is therefore timely to provide a brief appraisal of the status of modelling and of its relevance to reactor design. To identify the issues of long-term reactor significance it is convenient to revert to simple physical descriptions of the boundary plasma.

4.1 Power Loading of Divertor Targets

The assumption that energy convection through the plasma sheaths at the divertor target is the dominant sink of plasma energy leads to the following expression for the scale-length Δ_E of energy flow within the scrape-off layer around a circular cross section plasma:

$$\Delta_E \sim \left(\frac{2\pi R q \chi_\perp}{\delta_t}\right)^{1/2} \left(\frac{2kT_t}{m}\right)^{-1/4} . \qquad (4.1)$$

Here $\chi_\perp$ is the transverse thermal diffusivity, $(\delta_t kT_t)$ is the amount of energy carried across the sheath by each electron-ion pair of the divertor plasma whose temperature is $kT_t = kT_e = kT_i$ at the sheath edge, the ion mass is m, R is the major radius and q the safety factor. Typically $\Delta_E \sim$ (few cm) for INTOR and so the target [of effective area $2\pi R\Delta_E (\sin\alpha)^{-1}$] must be inclined at angle α to the magnetic surfaces in order to reduce the power loading at the surface to ~ 5 MW/m^2. It is apparent from Eq. (4.1) that Δ_E is rather insensitive to the plasma parameters but the present detailed models show that the peaking factor of the power load is quite sensitive to $\chi_\perp$ and to the magnetic topography. The models use prescribed values of $\chi_\perp$ which are in approximate accord with the magnitudes determined by experiment

(thermal diffusivity ranging from 1 to 5 m^2/s). The assumed radial dependences of $\chi_\perp$ range from invariant to Bohm-like and to Alcator /INTOR-like. There is no satisfactory experimental guide to this selection. Present uncertainty in the magnitude of $\chi_\perp$ may introduce a factor of about 2 into the peak power load whereas uncertainties in the radial dependence of $\chi_\perp$ have but slight effect.

Present plasma edge models used for NET and INTOR neglect interactions between the drifting boundary plasma and the magnetic field[14]. One significant omission[15] is the toroidal electric field which arises due to diffusion of electrons towards the hotter regions of the scrape-off plasma. In a crude sense such effects can be included by appropriate adjustment of the values of $\chi_\perp$ indeed they may contribute to the values derived from experiments. However, these interactions are sensitive to plasma collisionality and so caution must be exercised when accepting values of $\chi_\perp$ derived from weakly collisional experiments. Moreover, interactions between the edge plasma and the magnetic field are likely to introduce both toroidal and poloidal asymmetries into the effective $\chi_\perp$. These are presently neglected.

Plasma transport in the direction parallel to the magnetic field is assumed to be classical. Parallel electron thermal conductivity ($\kappa_\parallel^o T^{5/2}$) in a collisional scrape-off layer establishes a temperature gradient which for the preceding idealised plasma is of the form

$$Q_t = \frac{4}{7} \kappa_\parallel^o \frac{(T_s^{7/2} + T_t^{7/2})}{(\pi R q + L_d)} \left(\frac{2\pi a_s \Delta_E}{q}\right). \qquad (4.2)$$

The transverse flow of plasma power, $Q_\perp$, into the scrape-off is here assumed to be equally distributed to the inner and outer divertor targets (i.e. $2Q_t = Q_\perp$), the subscript "s" denotes conditions at the location of flow symmetry in the scrape-off layer, L_d is the distance (along the magnetic field) from the divertor throat to the target and a_s is the minor radius of the circular plasma. In practice $(T_s - T_t)$ is reduced significantly by plasma convection along the magnetic field. Experimental support for this physical picture is quite good but the implicit assumption of collisionality in a reactor becomes less valid in plasma regions adjacent to the sheath edge. There is evidence from the weakly collisional boundary of ASDEX[16] that the effective conductivity is less than the Spitzer value. This could reduce somewhat the

asymmetry of power flow reported here for the inner and outer targets. Nevertheless, it is not likely to increase the peak temperature at the outer target and it will only slightly raise the temperature T_s in the scrape-off.

Prescription of appropriate values of δ_t in Eq.(4.1) is based entirely upon classical theory. In this case the physics issues are better understood, but even so the influence of the long range quasi-collisional region of the pre-sheath has not been adequately explored. The enhancement of δ_t due to emission of secondary electrons from the target is neglected in NET/INTOR calculations because of the glancing angle at which the field intersects the divertor target. Measurements on DITE (see for example Ref. 17) provide some support for the theoretical value of $\delta_t \sim 8$ for D/T ions.

In principle the safety factor in Eq.(4.1) which is applicable close to the target can be determined precisely from the magnetic equilibrium contours. The detailed information is available for NET II but it has not yet been incorporated into the models. Thus the present results are based upon rather imprecise data taken from the INTOR reports. The ratio (B_{pol}/B_{tor}) is taken as 1/11.25 at both the outer and inner targets. The precise values for NET II are 1/5.9 and 1/9.9 for the outer and inner targets respectively. This implies that the reported power load on the outer target is underestimated by about a factor 2. This is not an inherent source of error but the discrepancy in the reported results should be noted.

Neglecting inconsistencies in the assumed values of B_{pol}/B_{tor}, it is reasonable to accept that the power loading can be predicted to a factor of about two and that the present results (for which $\chi_\perp \sim 2m^2/s$) lie in the upper range.

4.2 Plasma Temperature at the Sheath and Release of Sputtered Target Material

Assumption of the preceding simple plasma conditions leads to an expression for T_t, namely that

$$T_t \propto \left(\frac{Q_\perp}{n_s T_s \delta_t \Delta_E}\right)^2. \qquad (4.3)$$

Atomic power losses are neglected in Eq.(4.3) but this is not seriously

unrealistic in reactor conditions. It is evident that the plasma temperature close to the divertor target depends strongly upon the parameters in Eq.(4.3). The most precisely known of these are Δ_E and the scrape-off plasma temperature T_s. Confidence in the magnitude of T_s is due to the strong temperature dependence of parallel electron thermal conductivity [as can be seen in Eq.(4.2)]. Accepting that the divertor is moderately effective at retaining sputtered tungsten implies that $Q_\perp$ ranges only between about 50 and 80 MW. Greatest uncertainty arises due to the density n_s and it is compounded (a) from uncertainties in the radial diffusion coefficient $D_\perp$ and (b) from uncertainties in the radial flux of ions, $\Gamma_\perp$, because

$$\Gamma_\perp \sim D_\perp \frac{dn_s}{dr} . \qquad (4.4)$$

Clearly the upper limit must be compliant with $\langle n \rangle \sim 1.4 \times 10^{20}/m^3$ in NET/INTOR but the lower limit depends upon the balances between fuelling, particle exhaust and first wall recycling. For the present impurity control concept, the lowest acceptable value of n_{sx} (i.e. n_s at the separatrix) is $\sim 3.5 \times 10^{19}/m^3$ and it is governed by the onset of tungsten self-sputtering. The impact of H-mode operation is not clear. If the fundamental requirement of the edge plasma in this mode is to preclude the entry of charge exchange atoms across the separatrix then the H-mode in NET/INTOR could possibly be attained with $n_{sx} \sim 6$ to $7 \times 10^{19}/m^3$.

Choice of divertor target material is strongly influenced by the plasma temperature T_t. When the density n_{sx} during the steady state burn phase of NET/INTOR is $\sim 5 \times 10^{19}/m^3$, then (if tungsten is chosen as target material) the maximum electron temperature at the outer target is $T_t \lesssim 30$ eV. The incident energy of D/T ions then lies below the sputtering threshold for tungsten. A small amount of sputtering ($\sim 2 \times 10^{19}$ W atoms/s) occurs due to He^{2+} ions and possibly a smaller amount due to small concentrations of O and Fe impurities. The erosion profile is strongly peaked and deliberate scanning of the plasma over the target (as discussed in Section 2.7) might ensure an almost unlimited operational lifetime of the surface material. In these low sputtering conditions neither the efficacy of the divertor to retain sputtered impurities nor the inward transport of impurities into the hot central plasma are critical issues. They become increasingly important if

operation at lower values of n_{sx} is unavoidable. In this context, studies of impurity release during start-up, shut-down and during a low density phase of current drive (for transformer recharging) have not yet been undertaken. It should however be noted that Eq.(4.3) indicates that T_t tends to be invariant with the ratio $(Q_\perp/n_s)$.

The temperature T_t is also sensitive to the reflection of particle energy from the target. The model uses theoretical (TRIM code) data for the reflection coefficient R_E which for D/T ions on tungsten is ~ 0.8 over the energy range of interest. These data refer to an ideally smooth surface and moreover they have not been confirmed because there are no measurements for low energy particles. Small scale surface roughness is expected to cause a significant reduction in R_E because the incident particle can then participate in several momentum exchanging collisions before being truly backscattered. If such rough surface conditions pertain in a reactor, then the present calculations overestimate tungsten sputtering and a lower limit of n_{sx} would be acceptable.

If the target is made from low atomic number materials such as Be then T_t lies well above the sputtering threshold, moreover $R_E \sim 0.3$ so that evocation of surface roughness provides little amelioration of the sputtering problem. Sputtering rates can be predicted with greater confidence but this shows only that they are $\sim 10^2$ larger than for tungsten. Detailed knowledge of impurity retention within the divertor and inward transport to the main plasma then become critical links in any prediction of the contribution to β arising from low Z contamination. The sputtering release rate is so high that target lifetime is acceptable only if redeposition takes place without significant particle displacement. If the divertor plasma is continuously scanned over the target then the present uncertainties in the spatial distribution of redeposited particles are effectively bypassed and the overall erosion problem reduced somewhat.

There remain a number of unresolved questions relating to the basic aspects of sputtering at glancing incidence but, for low energy ions, this lack of knowledge is not likely to cause serious underestimation of the sputtering rates. The radial properties of the plasma sheath, which arise due to the presence of a very inhomogeneous divertor plasma, have not be explored. Nevertheless, the present estimates of sputtering should not be substantially changed due to this effect.

4.3 Exhaust of Neutral Gas and Erosion of Divertor Chamber Walls

Neutral particle transport can be modelled with quite high precision using Monte Carlo techniques and experimental results from ASDEX and PDX are compatible with the predicted performance. A higher level of consistency should be sought between the D/T plasma model and the source terms calculated by Monte Carlo methods, but this is not an inherent cause of error.

The major cause of error lies in the inconsistent treatment of helium ion transport both across and along the magnetic field (and possibly the transport of higher Z impurity ions). The greatest impact of this uncertainty is likely to be seen in the prediction of vacuum pumping requirements. Understanding of this issue is inadequate, but the tenuous evidence implies that the helium pumping speed might prudently be increased by a factor of 2 to 5.

Greater knowledge of the distribution of charge exchange atom damage of the first wall should be sought by extending the Monte Carlo calculations so that they at least embrace the lower region of first wall and divertor throat.

5. Conclusions

Improved modelling of both plasma and neutral particle transport has confirmed the concept that the open-throated, single-null poloidal divertor of NET/INTOR will readily operate in the high recycling regime. Power loading at the targets can be accommodated within the available space by suitable inclination to the magnetic surfaces even though the loading at the outer target is predicted to be about twice that at the inner. Impurities released at the first wall are likely to drift into the divertor chamber, but helium diffusing across the separatrix may encounter some degradation of exhaust efficiency until it has diffused into the outer half of the scrape-off plasma. It would thus be prudent to upgrade the vacuum pumping requirements for helium.

The analysis also confirms the choice of tungsten as a target material. Sputtering, which arises only due to the He^{2+} component of the incident plasma, causes a peak erosion of 2mm/y (100% availability) but uncontrolled motion of the divertor channels is likely to cause a substantial reduction. The concept of deliberatley scanning the plasma over the target would be beneficial in limiting erosion. It would also

bypass present uncertainties in the spatial distribution of redeposited target material.

Erosion of the stainless steel wall in between the pumping ducts is unacceptable but the problem could be eliminated by the use of tungsten armour.

Pumping performance can be optimised by restricting the height of the pumping ducts to 0.2 to 0.3 m.

There is reasonable experimental support for the trends predicted by these models, but in the context of NET/INTOR the least certain aspect in modelling is the density of plasma close to the separatrix of the scrape-off.

References

1. M.F.A. Harrison and E.S. Hotston (1982) in "European contributions to the INTOR-Phase IIA Workshop", Euratom, EUR FU BRU/XII-132/82/EDV30, Brussels (1982), Vol.2, p.VI-199.
2. International Tokamak Reactor Phase Two A, Part 1, IAEA, Vienna (1983), p.746.
3. P.J. Harbour, Nucl.Fusion, 24: 1211 (1984).
4. E.S. Hotston and M.F.A. Harrison - private communication.
5. B.J. Braams, in "11th European Conf. on Controlled Fusion and Plasma Physics", Aachen, Sept.1983, EPS 7D, Part II, p.431.
6. B.J. Braams, M.F.A. Harrison, E.S. Hotston and J.G. Morgan, in "European Contribution to the 8th Workshop-Meeting of INTOR Phase IIA", Euratom, EUR FU BRU/XII-1/84-EDV10 (1984).
7. M.F.A. Harrison, E.S. Hotston, A. De Matteis and J.G. Morgan, in "European Contributions to the 9th Workshop-Meeting of INTOR Phase IIA", Euratom, EUR FU BRU/XII-1/84/EDV20, Brussels (1984)
also
B.J. Braams, M.F.A. Harrison, E.S. Hotston and J.G. Morgan in "10th Int. Conf. on Plasma Physics and Controlled Nuclear Fusion Research", London, Sept. 1984, IAEA, Vienna, paper E-II-5-3.
8. M.F.A. Harrison and E.S. Hotston, in "European Contributions to the 10th Workshop-Meeting of INTOR Phase IIA", Euratom, EUR FU BRU/XII-1/84/EDV30, Brussels (1984).
9. E. Cupini, A. De Matteis, R. Simonini, E.S. Hotston and M.F.A. Harrison, NET Report 26, Euratom, EUR XII 324/26 (1984).
10. J. Neuhauser, W. Schneider, R. Wunderlick and K. Lackner (1984) in "European Contributions to the 10th Workshop-Meeting of INTOR Phase IIA" Euratom, EUR FU BRU/XII-1/84/EDV30, Brussels (1984).
11. W.J. Goedheer, in "European Contributions to the 10th Workshop-Meeting of INTOR Phase IIA", Euratom EUR, FU BRU/XII-1/84/EDV30, Brussels (1984).
12. E. Cupini, A. De Matteis and R. Simonini, NET Report 9, Euratom, EUR XII-324/9 (1983).
13. W. Eckstein, in "European Contributions to the 9th Workshop-Meeting of INTOR Phase IIA", Euratom, EUR FU BRU/XII-1/84/EDV20, Brussels (1984).

14. C.E. Singer, in "Physics of Plasma-Wall Interactions in Controlled Fusion", ed. R. Behrisch and D.E.Post, NATO ASI, Val-Morin, Canada, (1984) - to be published by Plenum Press.
15. W Feneberg, JET Laboratory, Working Note, JDN/T(84)19 (1984).
16. K. Lackner, B. Braams, R. Chodura et al, in "10th International Conference on Plasma Physics and Controlled Nuclear Fusion Research", London, September 1984, IAEA, Vienna, Paper A-V-4.
17. G. Proudfoot and P J Harbour, J.Nucl.Mater. 111 and 112:44(1982).